Mathematical Structures and Modeling
2022. N. 4 (64). PP. 60–74

UDC 532.5
DOI 10.24147/2222-8772.2022.4.60-74

ANALYSIS OF VORTEX-INDUCED FORCES ON THE GROUP OF SUBSEA STRUCTURES IN PROXIMITY OF EQUIPMENT AT RE=3900

H.F. Annapeh[1]
Laborant, Laboratory of Vibration and Hydrodynamics Modelling,
e-mail: kinghenry939@gmail.com
V.A. Kurushina[1,2]
Ph.D. (Eng.), Head of Laboratory of Vibration and Hydrodynamics Modelling; Research Associate, e-mail: v.kurushina@outlook.com

[1]Industrial University of Tyumen, Tyumen, Russia

[2]Newcastle University, Newcastle upon Tyne, United Kingdom

Abstract. Fluctuations of fluid forces associated with the vortex formation process are evaluated in this work for a group of subsea pipelines, placed in proximity of a larger piece of the subsea equipment and subjected to uniform and non-uniform flows. The computational fluid dynamics (CFD) simulations are performed for the average Reynolds number of 3900 with the k-ω SST turbulence model. Three different positions for the smaller staggered cylinders are considered, and the studied flow profiles are the uniform, linearly sheared and parabolic sheared flows. Simulation results include time histories of the hydrodynamic coefficients, FFT results, pressure on the smaller structures, velocity fields. Results for the parabolic sheared flow in the cases considered show an increase of mean drag coefficients, increase of amplitudes of the fluctuating drag and lift coefficients compared to values observed for the uniform flow and linearly sheared flow.

Keywords: vortex-induced forces, uniform flow, sheared flow, staggered cylinders, subsea pipelines, hydrodynamic coefficients.

1. Introduction

Vortex-induced forces contribute substantially to the fatigue damage and shortening the operational lifespan of slender subsea structures, including pipelines and risers conveying oil and gas from the seabed to the sea surface. Extracting the natural resources in deep waters implies an increased complexity of installations and repairs, partly due to the challenge of predicting correctly the hydrodynamic loads across long spans of structures suspended in medium and subject to various flows.

The well-known review work [1] studied both the flow over a single circular structure and the flow around two identical circular cylinders in tandem. This

study identified three flow regimes based on the center-to-center spacing ratio L/D (where L is the distance between centers of cylinders and D is the cylinder diameter). This work identified three main vortex shedding regimes around tandem structures, starting with the extended-body regime at $1.0 < L/D < 1.8$, where the wakes of two structures merge due to the structural proximity and lead to the formation of a single vortex street. The reattachment regime at $1.8 < L/D < 3.8$ was revealed by observing the shear layers detaching from the upstream cylinder and reattaching to the face of the downstream cylinder. In this case, the vortex shedding occurs only in the wake of the downstream cylinder. The co-shedding regime, where two separate vortex streets were forming, was observed at $L/D > 3.8$. This work laid a strong foundation for future investigations for the flow over a group of structures.

The method of computational fluid dynamics (CFD) is one of the main approaches to numerical simulations of the vortex formation process, where estimates of the pressure and fluid forces fluctuations are required. This method provides the maximum results accuracy if the approach of direct numerical simulations (DNS) is taken. For turbulence simulations at a high Reynolds number (Re), methods of large eddy simulations (LES) and Reynolds-averaged Navier-Stokes simulations (RANS) are often recommended in order to simplify the turbulent pulsations and improve the time efficiency. The work [2] studied the applicability of LES for high Reynolds number flows over a circular cylinder. It is worth noting numerical investigations using three-dimensional DNS and LES for a flow around a circular cylinder at Reynolds numbers of Re = 60–1000 in [3] and simulations on two tandem circular cylinders at subcritical Reynolds numbers in [4]. It is also worth noting the experimental studies in [5] for two staggered cylinders in turbulent flow, in [6, 7] - for three and four flexible cylinders and in [8] - for four squared cylinders at low Reynolds numbers.

Following the published results, the present work attempts to consider a flow over a group of stationary circular structures arranged in proximity to a larger structure, which would correspond to a realistic scenario of fluid loads and the vortex formation for a system of subsea structures. The aim of this work is to investigate the hydrodynamic coefficients, pressure distribution and vortex shedding patterns when three identical staggered stationary circular cylinders are subjected to uniform, linearly sheared and parabolic sheared flow at a Reynolds number of 3900, using the CFD RANS approach.

This paper consists of the following sections. Section 1 provides a brief theoretical background on the topic. Section 2 gives an overview of the numerical method and considered cases. Section 3 shows results of this study, and section 4 provides conclusions for this work.

2. Numerical model

A system of three identical staggered stationary circular structures of diameter $d = 0.3$ m, representing an array of subsea pipelines, is considered in this study in proximity to a larger object. This larger piece of the subsea equipment is

simplified to a cylinder of a squared cross-section with a side equal to $D = 5d$. The full system of structures is considered in a rectangular fluid domain of the size of $30D$x$16D$, showed in Fig. 1(a). Computational fluid dynamics (CFD) simulations are performed in this work for three staggered arrangements of cylinders, where the group of three smaller structures has three different positions relatively the larger object, as illustrated in Figs 1(a)-(c): with the cylinder closest to the squared structure located on the level of the upstream edge, centered relatively the larger structure and centered relatively its' downstream edge. Distance between circular structures is assumed equal to L, with the $L/D = 0.6$. The same distance of L from the side of the squared cylinder to the centre of the closest smaller cylinder is assumed the same for all considered cases. The distance from the squared cylinder to the domain border is $G = 20d$ in the performed simulations. The flow is entering the domain from the inlet (left) boundary, the periodic and shadow conditions are used for the top and bottom boundary, and the right boundary is the outlet.

Nine cases in total are considered in this work, with three cases for each inlet flow type. The uniform flow of the Reynolds number 3900 is simulated in Cases 1, 2 and 3, corresponding to the illustrations in Figs 1(a)-1(c), where the position of the circular structures is varied in alignment with the squared cylinder. Cases 4, 5, 6 represent the same structural arrangements as in Cases 1, 2, 3, but subjected to linearly sheared flow, and the Case 6 is displayed in Fig. 1(d). The linearly sheared flow is defined with respect to the vertical coordinate y along the inlet, where $y = 0$ corresponds to the centre of the inlet side of the domain. The linearly sheared flow velocity $U(y)$ is defined based on the averaged flow velocity U_c corresponding to the $Re = 3900$ at the inlet central point:

$$U(y) = U_c - By, \tag{1}$$

where the gradient used is $B = 0.022\ s^{-1}$, and the maximum flow velocity corresponds to the bottom boundary, while the minimum flow velocity corresponds to the top boundary.

Cases 7, 8, 9 are designed in a similar manner: structural arrangements in Cases 1, 2, 3 are subjected to the parabolic sheared flow, and Case 9 is illustrated in Fig. 1(e). The velocity of the parabolic flow is defined for the inlet boundary using the total length of inlet $h = 16D$:

$$U(y) = U_c(1 - \left(\frac{2y}{h}\right)^2), \tag{2}$$

where the maximum flow velocity corresponding to the $Re = 3900$ is on the domain centreline.

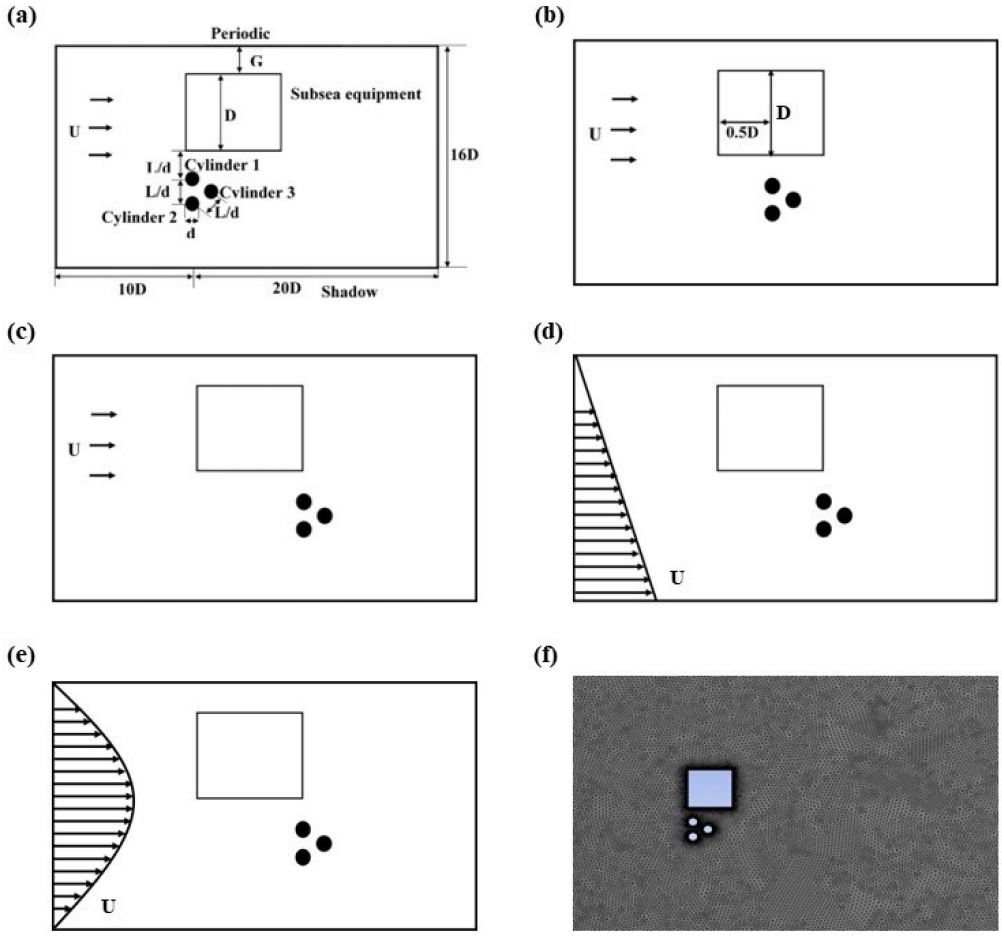

Figure 1. Computational domain for the considered cases: (a) Case 1 with staggered cylinders in uniform flow placed at the beginning of the square cylinder; (b) Case 2 with staggered cylinders in uniform flow placed exactly at the middle of the square cylinder; (c) Case 3 with staggered cylinders in uniform flow placed at the end of the square cylinder; (d) Case 6 with staggered cylinders in linearly sheared flow; (e) Case 9 with staggered cylinders in parabolic sheared flow; (f) Mesh of the computational domain for Cases 1, 4, 7.

Table 1: Mesh independence test results for $Re = 3900$

Cases	C_{D0}	**Number of cells**	y^+
Current study			
Mesh 1	0.87	31 297	0.0133
Mesh 2	0.91	53 951	0.0132
Mesh 3	0.93	86 637	0.0131
Mesh 4	0.93	153 227	0.0131
Published data			

LES [9]	0.92	–	–
Experiments [10]	0.98	–	–
VMS-LES [11]	0.99	–	–
LES [12]	0.98	–	–

Table 2: Simulation results

Cases	Hydrodynamic coefficients				
	C_{D0}	C_{D0}^{fl}	C_L	Dominant frequency, Hz	
				C_D	C_L
Uniform flow					
Cylinder 1					
Case 1	0.52	0.13	0.08	0.0015	0.0140
Case 2	0.47	0.12	0.02	0.0035	0.0125
Case 3	0.43	0.11	0.10	0.0020	0.0125
Cylinder 2					
Case 1	0.46	0.10	0.09	0.0015	0.0125
Case 2	0.42	0.11	0.05	0.0010	0.0125
Case 3	0.38	0.07	0.04	0.0020	0.0110
Cylinder 3					
Case 1	0.43	0.28	0.65	0.0015	0.006
Case 2	0.33	0.18	0.47	0.0125	0.004
Case 3	0.31	0.15	0.43	0.0070	0.003
Linearly sheared flow					
Cylinder 1					
Case 4	0.50	0.12	0.05	0.0020	0.0145
Case 5	0.43	0.15	0.03	0.0005	0.0125
Case 6	0.41	0.11	0.05	0.0035	0.1250
Cylinder 2					
Case 4	0.44	0.08	0.06	0.0050	0.0130
Case 5	0.39	0.12	0.04	0.0125	0.0120
Case 6	0.38	0.08	0.04	0.0010	0.0120
Cylinder 3					

Continued on next page

Cases	Hydrodynamic coefficients				
	C_{D0}	C_{D0}^{fl}	C_L	Dominant frequency, Hz	
				C_D	C_L
Case 4	0.43	0.28	0.64	0.0100	0.0050
Case 5	0.32	0.37	0.55	0.0125	0.0045
Case 6	0.34	0.30	0.53	0.0045	0.0040
Cases	Hydrodynamic coefficients				
	C_{D0}	C_{D0}^{fl}	C_L	Dominant frequency, Hz	
				C_D	C_L
Parabolic flow					
Cylinder 1					
Case 7	0.81	0.26	0.12	0.0030	0.0090
Case 8	0.71	0.25	0.04	0.0025	0.0080
Case 9	0.67	0.21	0.12	0.0080	0.0075
Cylinder 2					
Case 7	0.71	0.25	0.22	0.0090	0.0085
Case 8	0.64	0.09	0.13	0.0085	0.0080
Case 9	0.60	0.12	0.12	0.0075	0.0075
Cylinder 3					
Case 7	0.66	0.44	1.15	0.0095	0.0030
Case 8	0.49	0.39	0.78	0.0080	0.0025
Case 9	0.48	0.37	0.73	0.0075	0.0030

Simulations are performed using the 2D incompressible Navier-Stokes system of equations, k-ω SST turbulence model, PISO algorithm and the time step of 0.1 s. The triangular grid is used for simulation purposes, and the results for the mean drag coefficient C_{D0}, the fluctuating drag coefficient C_D^{fl} and the lift coefficient C_L are reported in the next section. Here, the total drag coefficient obtained during the simulations is $C_D = C_{D0} + C_D^{fl}$. The mesh independence test results are reported in Table 1 for the uniform flow of the Reynolds number of 3900 and the mesh shown in Fig. 1(f). Comparison with the results for the mean drag coefficient C_{D0} ensures a sufficiently accurate match to the values reported in [9–12]. Mesh 3 from Table 1 is selected for all calculations in this work.

3. Results and discussion

The summary of results obtained in this study for the nine cases is given in Table 2, and time histories of the fluctuating drag and lift coefficients together

with the corresponding FFT records are displayed in Figs 2-10.

The uniform flow simulations, illustrated in Figs 2-4, indicate a progressive decrease in the mean drag coefficient on each cylinder for all three cases, with the cylinder 1 experiencing the highest mean drag coefficient of about 0.52, as shown in Fig. 2. In all the three considered cases, the cylinder 3 experiences the least mean drag coefficient. Cylinder 3, placed downstream in the array, experiences the highest fluctuating drag coefficient and the maximum amplitude of lift coefficient in three cases considered. Low frequency fluctuations of fluid forces are indicated by results in Table 2, with clearly identified dominant frequencies. Stable oscillations observed after 500 s in Case 1, after 1500 s in Case 2 and after 300 s in Case 3.

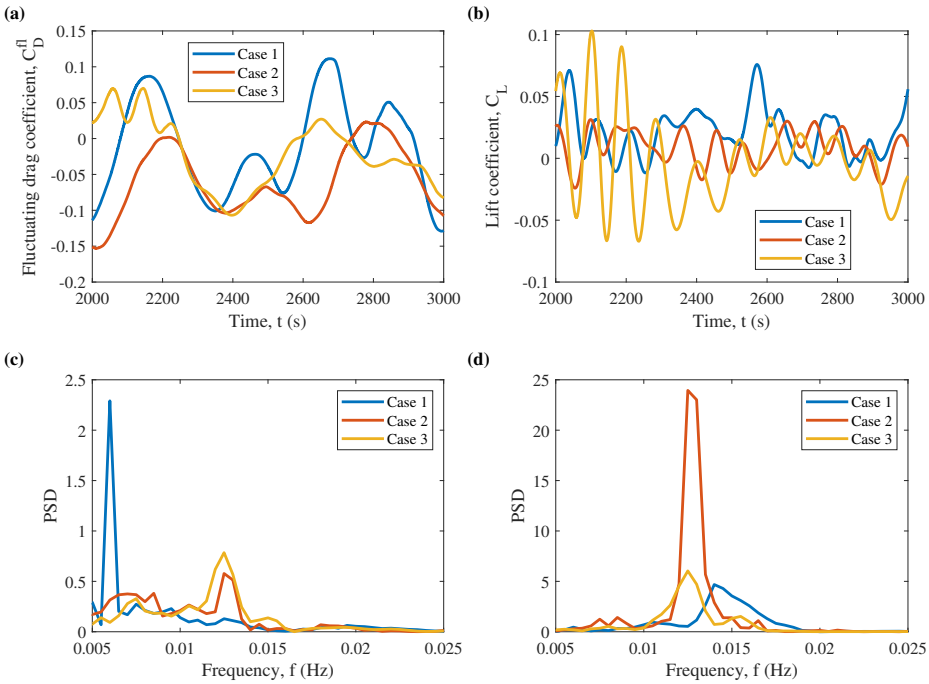

Figure 2. Fluid force coefficients for cylinder 1 immersed in the uniform flow: (a) time history of the fluctuating drag coefficient; (b) time history of the lift coefficient; (c) the fluctuating drag coefficient FFT; (d) the lift coefficient FFT.

For the linearly sheared flow, illustrated in Figs 5-7, there is a gradual decrease in the mean drag coefficient acting on each circular cylinder from Case 4 to 6. The cylinder 1, as shown in Fig. 5, experiences the highest mean drag coefficient in all three considered cases, and the cylinder 3 experiences the least mean drag coefficient. The highest fluctuating drag coefficient and the maximum amplitude of the lift coefficient signal is experienced by cylinder 3 in all the three considered cases, as appears in Fig. 7. Results for the linearly sheared current also confirm the low frequency fluctuations of fluid forces, experienced by all structures. Fluctuating drag coefficient signal for cylinder 3 demonstrates multiple frequencies and generally higher complexity of the signal than for other structures. The average drag coefficient acting on each cylinder in the uniform flow is generally higher than in the linearly sheared flow. The fluctuating drag coefficient for the linearly

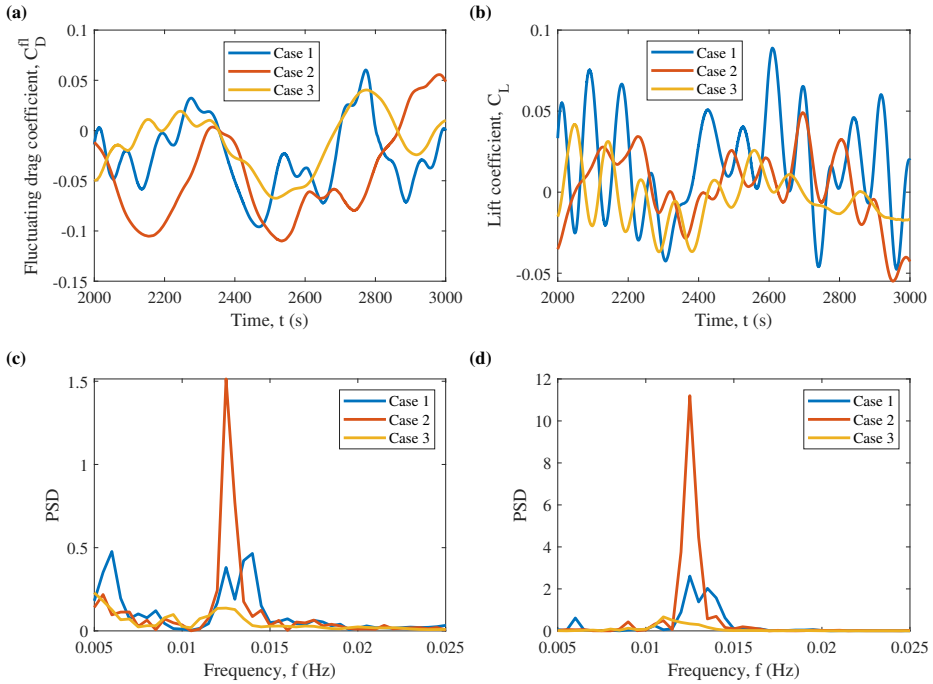

Figure 3. Fluid force coefficients for cylinder 2 immersed in the uniform flow: (a) time history of the fluctuating drag coefficient; (b) time history of the lift coefficient; (c) the fluctuating drag coefficient FFT; (d) the lift coefficient FFT.

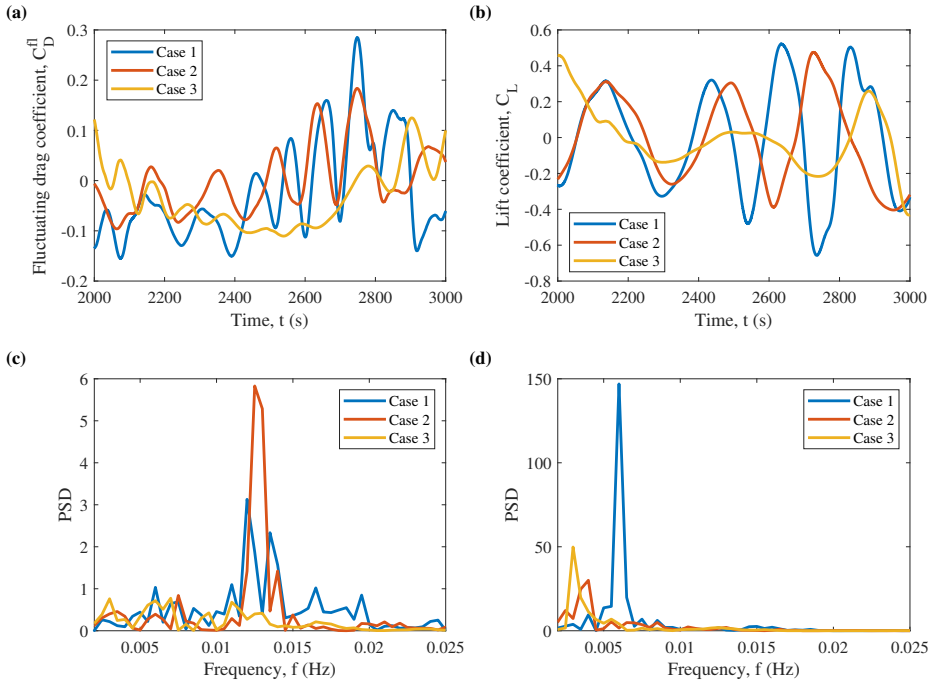

Figure 4. Fluid force coefficients for cylinder 3 immersed in the uniform flow: (a) time history of the fluctuating drag coefficient; (b) time history of the lift coefficient; (c) the fluctuating drag coefficient FFT; (d) the lift coefficient FFT.

sheared flow is also much higher than that of the uniform flow.

The mean drag coefficient acting on each cylinder decreases from Case 7 to 9

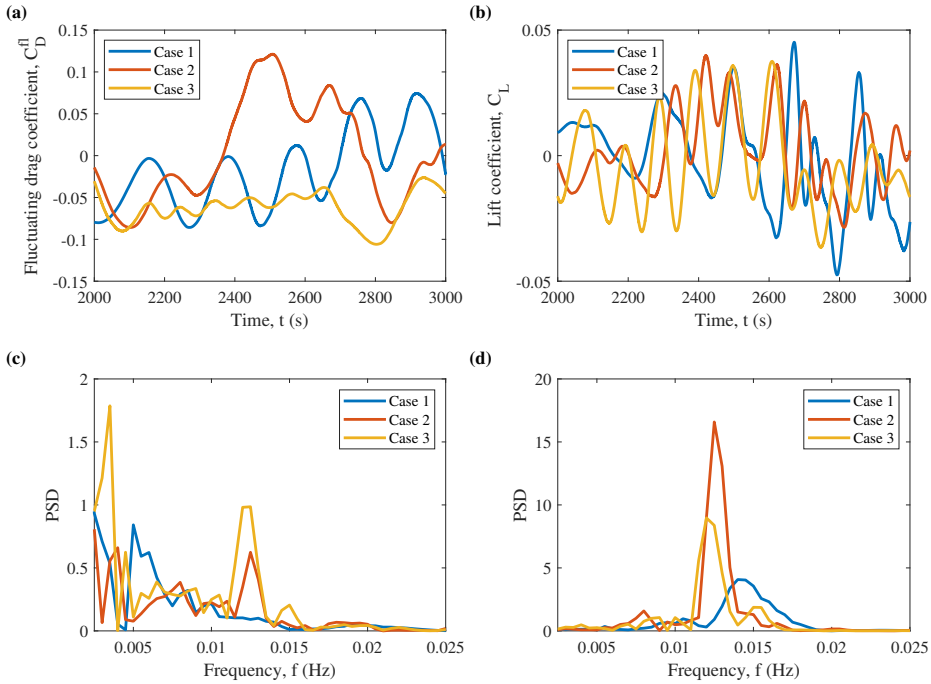

Figure 5. Fluid force coefficients for cylinder 1 immersed in the linearly sheared flow: (a) time history of the fluctuating drag coefficient; (b) time history of the lift coefficient; (c) the fluctuating drag coefficient FFT; (d) the lift coefficient FFT.

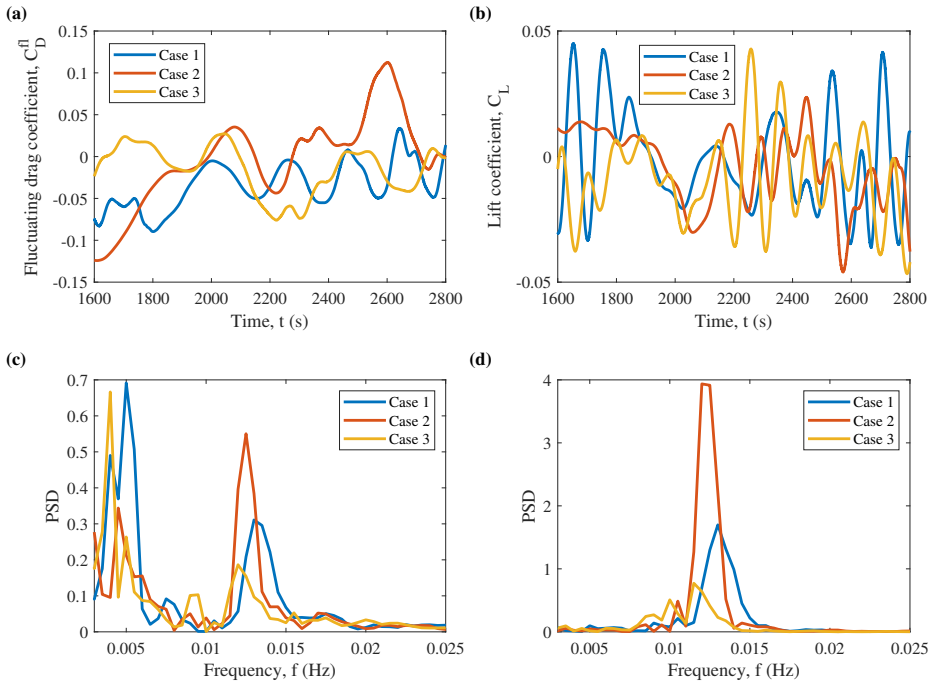

Figure 6. Fluid force coefficients for cylinder 2 immersed in the linearly sheared flow: (a) time history of the fluctuating drag coefficient; (b) time history of the lift coefficient; (c) the fluctuating drag coefficient FFT; (d) the lift coefficient FFT.

in the parabolic sheared flow, as displayed in Figs 8-10. Cylinder 1 experiences the highest mean drag coefficient of 0.81 in all the three considered cases, as

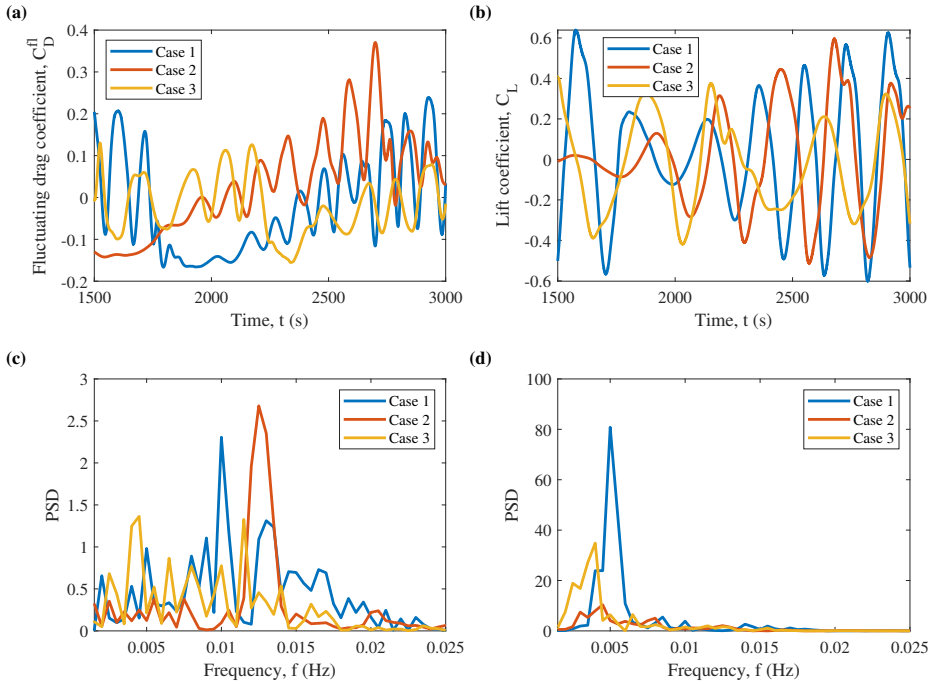

Figure 7. Fluid force coefficients for cylinder 3 immersed in the linearly sheared flow: (a) time history of the fluctuating drag coefficient; (b) time history of the lift coefficient; (c) the fluctuating drag coefficient FFT; (d) the lift coefficient FFT.

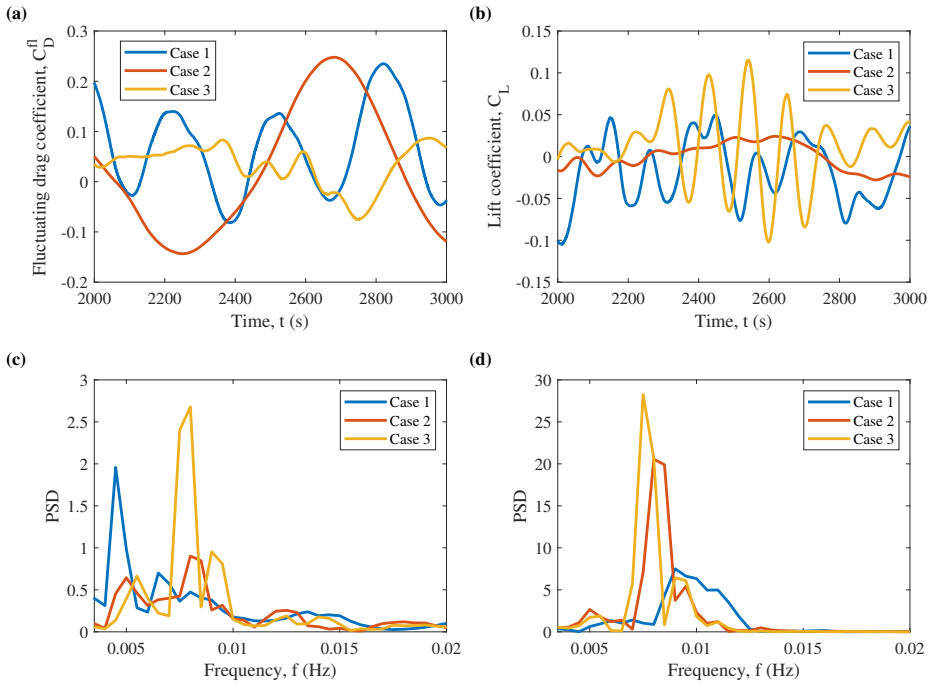

Figure 8. Fluid force coefficients for cylinder 1 immersed in the parabolic sheared flow: (a) time history of the fluctuating drag coefficient; (b) time history of the lift coefficient; (c) the fluctuating drag coefficient FFT; (d) the lift coefficient FFT.

demonstrated in Fig. 8. Cylinder 3 experiences the least mean drag coefficient of 0.48. The highest fluctuating drag coefficient and the maximum amplitude of

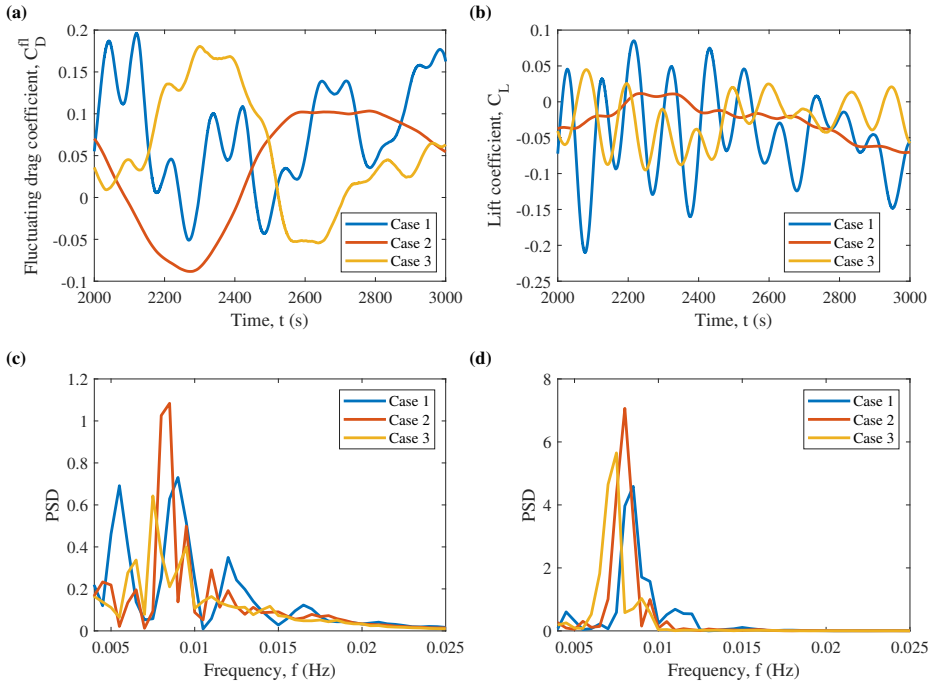

Figure 9. Fluid force coefficients for cylinder 2 immersed in the parabolic sheared flow: (a) time history of the fluctuating drag coefficient; (b) time history of the lift coefficient; (c) the fluctuating drag coefficient FFT; (d) the lift coefficient FFT.

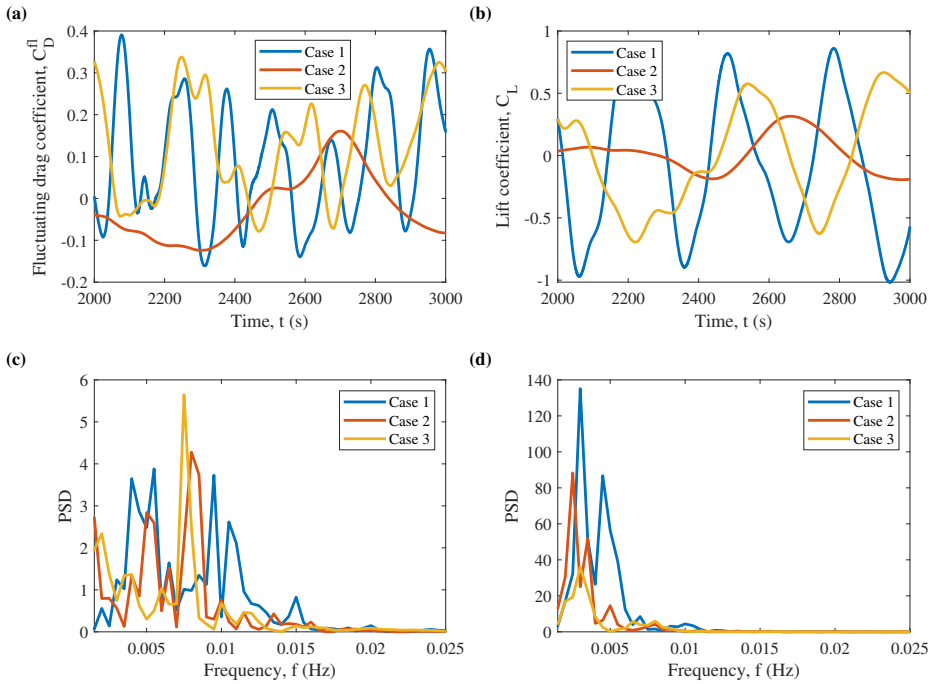

Figure 10. Fluid force coefficients for cylinder 3 immersed in the parabolic sheared flow: (a) time history of the fluctuating drag coefficient; (b) time history of the lift coefficient; (c) the fluctuating drag coefficient FFT; (d) the lift coefficient FFT.

the lift coefficient signal is experienced by cylinder 3 in all the three considered cases. Low frequency oscillations are consistent with the results for the uniform

and linearly sheared flow. However, the average drag coefficient acting on each cylinder for the parabolic sheared flow is higher than that of the linearly sheared flow and uniform flow. The fluctuating drag coefficient for the parabolic sheared flow is also much higher than that of the uniform flow and linearly sheared flow.

Case 8 with the medium position of the group of structures leads to the $2P$ vortex shedding from the group of smaller subsea structures, where three wakes merge into a single vortex street, as shown in Fig. 11(a). At the same time, a similar $2P$ vortex shedding regime is observed behind the squared cylinder. Vortex formation in this case occurs with similarly low shedding frequencies for both vortex streets, and the relative position of the group of smaller structures influences the difference in a phase of the vortex shedding cycle. For this reason, vortices shed from the smaller cylinders in a half-cycle towards the larger squared cylinder overlay and merge with vortices shed during one of the half-cycles of the squared cylinder. Vortices following the larger squared structure are, respectively, greater in size than vortices associated with the smaller structures. Two vortex streets in all considered cases merge into a single wake some distance past the set of structures considered.

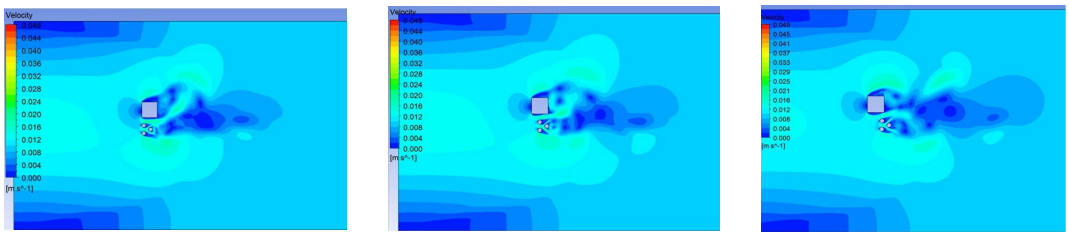

(a) (b) (c)

Figure 11. Velocity field indicating vortex shedding features: (a) Case 7; (b) Case 8; (c) Case 9.

In Cases 7 and 9, the squared structure demonstrates a rather asymmetric vortex shedding, while the group of smaller cylinders retains the $2P$ mode, as appears in Fig. 11. In Case 7, displayed in Fig. 11(b), the vortex street from the larger structure appears unstable during the simulation time with the shedding mode closer to $2P+2S$. The cylinder 2 periodically contributes a separate vortex to the vortex pair from the cylinder 3 with their further coalescence. The arrangement in Case 9 leads to an asymmetric shedding from the squared cylinder, illustrated in Fig. 11(c), where the half-cycle in the direction away from the group of circular cylinders produces a $P+S$ combination of vortices, while the following half-cycle results in a vortex pair that immediately merges with the vortex street from the smaller structures.

The pressure distribution along the circumference, in terms of the angle from the centreline parallel to the X axis, is displayed in Fig. 12 for three structures in different flow conditions and with respect to the angle Θ. Here, $\Theta = 0$ is the upstream point on the cylinder centreline. The pressure $P = 0$ corresponds to the

average pressure in the fluid away from structures. Fig 12(a) shows the distribution of the pressure along the surface of cylinder 1. Here, the magnitude of the pressure becomes zero at $\Theta = 121^o$ and $\Theta = 175^o$, while reaches its maximum positive value at $\Theta = 150^o$ (the stagnation point). The maximum negative values are observed at $\Theta = 81^o$ and $\Theta = 203^o$ for the uniform flow. For the linearly sheared flow, the magnitude of the pressure becomes zero at $\Theta = 120^o$ and $\Theta = 179^o$, reaches its maximum positive value at $\Theta = 150^o$, and reaches its maximum negative values at $\Theta = 85^o$ and $\Theta = 210^o$ and for the parabolic sheared flow the magnitude of the pressure becomes zero at $\Theta = 121^o$ and $\Theta = 182^o$, reaches its maximum positive value at $\Theta = 150^o$, and reaches its maximum negative values at $\Theta = 86^o$ and $\Theta = 212^o$.

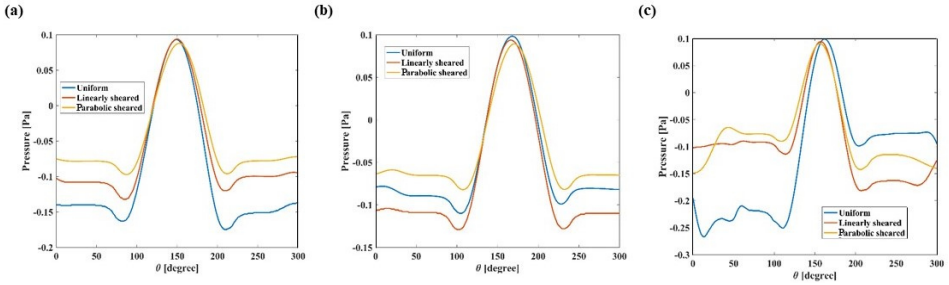

Figure 12. Pressure distribution on structures in Cases 3, 6 and 9, for three considered flow types, in comparison: (a) along cylinder 1, (b) along cylinder 2, (c) along cylinder 3.

4. Conclusions

Numerical simulations are performed in this work for three identical staggered stationary cylinders, forming an equilateral triangle, at the average Reynolds number of 3900. The structures are placed in a close proximity to a squared cylinder, representing a larger piece of the subsea equipment, and fluctuations of the vortex-induced forces are evaluated for the uniform, linearly sheared and parabolic sheared flow profiles. The k-ω SST turbulence model is used in order to obtain predictions for these nine cases for 3100 s of the physical time. Three different positions of the staggered circular cylinders relatively the larger structure are considered, and the hydrodynamic coefficients, pressure distribution around the cylinders, frequency of the drag and lift coefficient signals and vortex shedding patterns are obtained.

Among the cases considered, the least mean drag coefficient is registered for the cases 3, 6 and 9, for all velocity profiles. The larger mean drag coefficients, amplitudes of the fluctuating drag coefficient and lift coefficient are generally observed for the parabolic sheared flow profile. For each considered inlet velocity profile, cylinder 1, the closest to the piece of the subsea equipment, experiences effects from the drag force with the increased mean drag coefficient and amplitude of the fluctuating drag coefficient, as well as a larger amplitude of the lift force compared to the other two structures. Considered turbulent flows at the average Reynolds

number of 3900 lead to the very low frequency oscillations of both lift and drag coefficients, reflected in the slow process of the vortex formation. Results obtained in the current work generally continue the line of published research findings for the groups of four structures, located in proximity to each other.

Vortex streets in the wake from the group of smaller cylinders in the cases considered appear to combine into a single vortex street. At the same time, a separate vortex street with larger vortices appears to form in the wake of the squared structure. Future work in this direction should, therefore, focus on studying the effects from variation of distances among the structures, their relative sizes and positions in order to observe the evolution of vortex-induced forces and vortex formation processes.

Acknowledgments

The authors would like to acknowledge the support of the National Project "Science and Universities" of the Ministry of Science and Higher Education of the Russian Federation, grant number FEWN-2021-0012.

References

1. Zdravkovich M.M. Review of flow interference between two circular cylinders in various arrangements // ASME Journal of Fluids Engineering. 1977. No. 99. P. 618–633.
2. Breuer M. A challenging test case for large eddy simulation: High Reynolds number circular cylinder flow // International Journal of Heat Fluid Flow. 2000. No. 21. P. 648–654.
3. Shuyang C., Shigehira O., Yukio T., Yaojun G., Hironori K. Numerical simulation of Reynolds number effects on velocity shear flow around a circular cylinder // Journal of Fluids and Structures. 2010. No. 26. P. 685–702.
4. Xu W., Haokai W., Kun J., Enhao W. Numerical investigation into the effect of spacing on the flow-induced vibrations of two tandem circular cylinders at subcritical Reynolds numbers // Ocean Engineering. 2021. No. 236. P. 1-19.
5. Sumner D., Richards M.D., Akosile O.O. Two staggered circular cylinders of equal diameter in cross-flow // Journal of Fluids and Structures. 2005. No. 20. P. 255–276.
6. Wang E., Xu W., Yu Y., Zhou L., Incecik A. Flow-induced vibrations of three and four long flexible cylinders in tandem arrangement: An experimental study // Ocean Engineering. 2019. No. 178. P. 170–184.
7. Xu W., Zhang S., Ma Y., Liu B. Fluid forces acting on three and four long side-by-side flexible cylinders undergoing flow-induced vibration (FIV) // Marine Structures. 2021. No. 75. 102877.
8. Yuhang Z., Rui W., Yaoran C., Yan B., Zhaolong H., Dai Z., Huan P., Shixiao F., Yongsheng Z. Three-dimensional wake transition in the flow over four square cylinders at low Reynolds numbers // AIP Advances. 2020. No. 10. 015142.
9. Beaudan P., Moin P. Numerical experiments on the flow past a circular cylinder at a sub-critical Reynolds number, Report No. TF-62, Thermosciences Division, Department of Mechanical Engineering, Stanford University, USA, 1994.

10. Norberg C. Effects of Reynolds number and low-intensity free-stream turbulence on the flow around a circular cylinder, Publ. No. 87/2, Department of Applied Thermoscience and Fluid Mechanics, Chalmers University of Technology, Sweden, 1987.
11. Wornom S., Ouvrard H., Salvetti M. V., Koobus B., Dervieux A. Variational multiscale large-eddy simulations of the flow past a circular cylinder: Reynolds number effects // Computers and Fluids. V. 1, No. 47. P. 44–50.
12. Franke J., Frank W. Large eddy simulation of the flow past a circular cylinder at $Re = 3900$ // Journal of wind engineering and industrial aerodynamics. 2002. V. 10, No. 90. P. 1191–1206.

АНАЛИЗ ВИХРЕОБРАЗОВАТЕЛЬНЫХ СИЛ, ДЕЙСТВУЮЩИХ НА ГРУППУ ПОДВОДНЫХ КОНСТРУКЦИЙ ВБЛИЗИ ОБОРУДОВАНИЯ ПРИ RE=3900

Г.Ф. Аннапе[1]
Лаборант, Лаборатория вибрационного и гидродинамического моделирования„
e-mail: kinghenry939@gmail.com
В.А. Курушина[1,2]
Заведующий лабораторией, Лаборатория вибрационного и гидродинамического моделирования; научный сотрудник, e-mail: v.kurushina@outlook.com

[1]Тюменский индустриальный университет, Тюмень, Россия
[2]Университет Ньюкасла, Ньюкасл-на-Тайне, Великобритания

Аннотация. Колебания сил жидкости, связанные с вихреобразовательным процессом, оцениваются в данной работе для группы подводных трубопроводов, расположенных вблизи более крупного подводного оборудования и подверженных равномерному и неравномерному течению. Моделирование методом вычислительной динамики флюидов (CFD) производится для среднего числа Рейнольдса 3900 с помощью турбулентной модели k-ω SST. В работе рассмотрены три различных положения конструкций меньшего диаметра в шахматном порядке, и исследуются равномерный, линейно-неравномерный и параболический неравномерный профили потока. Результатами моделирования являются временная история колебаний гидродинамических коэффициентов, анализ частот FFT, данные по давлению на меньшие конструкции и данные по скорости потока. Результаты моделирования параболического нелинейного потока показывают увеличение среднего коэффициента гидродинамического сопротивления, рост амплитуд колеблющихся коэффициентов сопротивления и подъёмной силы, по сравнению с величинами, которые наблюдаются в равномерном потоке и линейном неравномерном потоке.

Ключевые слова: вихреобразовательные силы, равномерный поток, неравномерный поток, цилиндры в шахматном порядке, подводные трубопроводы, гидродинамические коэффициенты.

Дата поступления в редакцию: 02.11.2022